The metal–insulator transition in the half-filled extended Hubbard model on a triangular lattice



2009 J. Phys.: Condens. Matter 21 485702

(http://iopscience.iop.org/0953-8984/21/48/485702)

J. Phys.: Condens. Matter **21** (2009) 485702 (9pp) doi:10.1088/0953-8984/21/48/485702

# The metal–insulator transition in the half-filled extended Hubbard model on a triangular lattice

**Jiming Gao**[1,2] **and Jiaxiang Wang**[1]

[1] State Key Laboratory of Precision Spectroscopy and Department of Physics, East China Normal University, Shanghai 200062, People's Republic of China
[2] College of Physics and Electronic Engineering, Northwest Normal University, Lanzhou 730070, People's Republic of China

E-mail: jxwang@phy.ecnu.edu.cn

Received 25 August 2009, in final form 10 August 2009
Published 30 October 2009
Online at stacks.iop.org/JPhysCM/21/485702

**Abstract**

In this paper, we have investigated the metal–insulator transition (MIT) in a two-dimensional half-filled extended Hubbard model on an isotropic triangular lattice with a real space block renormalization group technique. It has been found that the MIT can be driven nontrivially by either the on-site interaction $U$ or the nearest-neighbor one $V$, but with different critical exponents. Depending upon the values of $V$, the system could have one, two or three MIT critical points. Moreover, for the metallic regime, we have also studied the competition effect from the spin density wave and charge density wave phases by using a mean-field theory based upon Hartree–Fock approximations. Finally, the single-site entanglement is also calculated and its first derivative with respect to $U$ shows a jump along the critical line of the MIT.

## 1. Introduction

The metal–insulator transition (MIT) is one of the central problems in condensed matter physics. Ever since the experimental discovery of metal states in 2D electronic systems [1], the influence of the interplay among disorders, electron interactions and geometric structures upon the MIT has been a subject of intense studies [2]. In particular, the competition between interactions and geometric frustrations can result in a wide range of exotic phases, which has attracted a lot of attention [3]. The triangular lattice is one of the prime examples having a frustration structure and can be found in a lot of materials, such as $NiGa_2S_4$ and organic compounds of $\kappa$-$(BEDT\text{-}TTF)_2Cu_2(CN)_3$ [4]. The phase transitions in those materials are closely connected to the electronic correlations and the geometric frustrations.

The Hubbard model (HM) [5] is the minimal model having electron interactions. The early results show that the ground state of a half-filled HM on a square lattice is a Mott insulator with Néel order for all positive values of $U/t$. In comparison, a frustrated triangular lattice has been shown to support a nontrivial MIT at finite interactions by various numerical calculations, for example, exact diagonalizations [6], mean-field resonating-valence-bond calculations [7] and the real space renormalization group (RSRG) method [8]. This clearly demonstrates the critical role played by the combined effects of interactions and geometric frustrations in the MIT. But the interactions in the normal HM only involve on-site interactions. So what will happen if nearest-neighbor interactions are included? The answer to this question will not only have fundamental theoretical interest, but also have great experimental relevance due to the discovery of many new materials, such as triangular lattice antiferromagnets of the $CuCrO_2$ family and transition-metal oxide materials $Na_xCoO_2$ and $Na_{1-x}TiO_2$ [9, 10]. These materials are characterized by rich kinds of charge and spin orders, which are believed to be related to the long-range interactions. In this paper, we will try to answer the above question through use of the extended Hubbard model (EHM) on a triangular lattice, which includes both nearest-neighbor interactions and a frustration structure.

The 2D EHM is a typical many-body model. It is almost impossible to obtain an analytical solution. We have to resort to approximations and numerical calculations, such as Monte Carlo simulation [11], exact diagonalization [12], renormalization group (RG) techniques [6, 13] and self-consistent mean-field approximation [14, 15]. Tsai, Marston [16] and Honerkamp [17] investigated the superconducting instability on the

 

2D triangular lattice by RG techniques. Recently, Davoudi has studied the EHM by a two-particle self-consistent approach for the density and the interaction-dependent crossover diagram for spin density wave (SDW) and charge density wave (CDW) instabilities of the normal state. In our work, we will make use of the real space block renormalization group (RSBRG) method for the solution. This method has already been successfully applied in the study of the MIT in the HM on a triangular lattice [18], which gives us great confidence in extending it to the EHM. The advantages of the RSBRG are that it can directly give the charge gap, the order parameter of the MIT, and also the single-site entanglement, which has been shown to represent some inherent many-body correlations and can be regarded as a general reference order parameter for quantum phase transitions [19], independent of the underlying driving mechanism. Besides the MIT, a self-consistent Hartree–Fock approximation (HFA) is also used to study the CDW and SDW phase transitions in the EHM.

This paper is organized as follows. In section 2, the Hamiltonian and the methods of the RSBRG and the HFA are introduced. Section 3 presents the detailed numerical results and the discussion. Finally, a brief summary is given in section 4.

## 2. The model and methods

The extended Hubbard model is defined by the Hamiltonian

$$H = -t \sum_{\langle i,j\rangle,\sigma} [c^{\dagger}_{i\sigma} c_{j\sigma} + \text{h.c.}] + U \sum_i n_{i\uparrow} n_{i\downarrow} + V \sum_{\langle i,j\rangle} n_i n_j - \mu \sum_i n_i \tag{1}$$

where $t$ is the nearest-neighbor hopping term, $U$ the local repulsive interaction, $V$ the nearest-neighbor Coulomb interaction and $\mu$ the chemical potential. $c^{\dagger}_{i\sigma}$ ($c_{i\sigma}$) creates (annihilates) an electron with spin $\sigma$ in a Wannier orbital located at site $i$. $n_{i\sigma}(=c^{\dagger}_{i\sigma}c_{i\sigma})$ is the number operator and $n_i = (n_{i\uparrow} + n_{i\downarrow})$. $\langle\,\rangle$ denotes the nearest-neighbor pair and H.c. means Hermitian conjugate. For a half-filled system, based upon particle–hole symmetry, equation (1) can be rewritten as

$$H = -t \sum_{\langle i,j\rangle,\sigma} [c^{\dagger}_{i\sigma} c_{j\sigma} + \text{h.c.}] + U \sum_i (\tfrac{1}{2} - n_{i\uparrow})(\tfrac{1}{2} - n_{i\downarrow}) + V \sum_{\langle i,j\rangle} (1 - n_i)(1 - n_j) + k \sum_i I_i, \tag{2}$$

where $\mu = U/2 + 6V$, $k = -(U/4 + 6V)$ and $I_i$ is the unit operator.

### 2.1. The block renormalization group

For a many-body Hamiltonian, due to the huge size of the Hilbert space, it is usually very hard to obtain its eigenvalues and eigenvectors. But when the microscopic spatial fluctuations are not very important for the physical results, we can follow Kadanoff's idea [20] of using the block renormalization group (BRG) method by dividing the lattice into blocks. Each block is then taken as an effective site of a new lattice. The hopping terms on the new lattice are evaluated by averaging over the interblock interactions. Repeating this procedure, we can get the so-called fixed point in the parameter space.

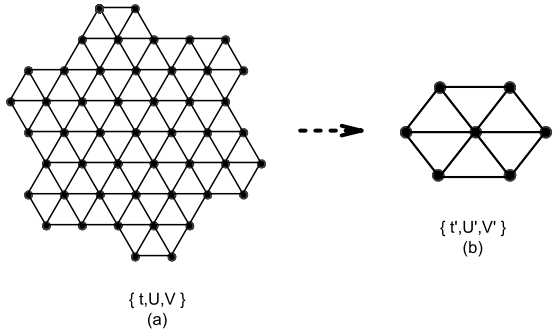


**Figure 1.** Schematic diagram for the procedure of the real space block renormalization group method applied in the EHM. (a) shows the original triangular lattice with parameters $\{t, U, V\}$ and (b) presents the new lattice with renormalized parameters $\{t', U', V'\}$ after mapping each hexagonal block into one effective site.

Mathematically, the procedure starts by decomposing the Hamiltonian into two parts:

$$H = \sum_b H_b + \sum_{\langle b,b'\rangle} H_{b,b'}, \tag{3}$$

where $b = 1, 2, \ldots, N/n^s$ is the block label with $N$ and $n^s$ the size of the lattice and the block, respectively. $H_b$ represents the block Hamiltonian and $H_{b,b'}$ the interblock interactions. $H_b$ can be solved numerically with eigenvalues $\lambda_{b,i}$ and eigenvectors $|\varphi_{b,i}\rangle$, from which we can build a complete set of new bases of the whole system, $|\Psi\rangle = |\varphi_{1,i_1}\rangle|\varphi_{2,i_2}\rangle \ldots |\varphi_{N/n^s,i_{N/n^s}}\rangle$. In this new set of basis, $H$ can be formally rewritten as

$$H = \sum_{\Psi,\Psi'} |\Psi\rangle\langle\Psi|H|\Psi'\rangle\langle\Psi'|. \tag{4}$$

Until now, everything has been exact and the new Hamiltonian is spanned in a Hilbert space of the same size as the original one. The next important step is to truncate the Hilbert space in a proper way. In the BRG method, the low-lying energy states of the block are often taken. Considering the fact that the Hilbert space dimension for each site is 4, we will keep only four block states in order to guarantee a similar structure connecting the renormalized and the old Hamiltonians.

On the basis of the above general rule, in our work, we divide the triangular lattice into blocks of seven sites, as shown in figure 1. The block Hamiltonian is

$$H_b = -t \sum_{\langle i^{(b)}, j^{(b)}\rangle,\sigma} [c^{\dagger}_{i^{(b)}\sigma} c_{j^{(b)}\sigma} + \text{h.c.}] + U \sum_{i^{(b)}} (\tfrac{1}{2} - n_{i^{(b)}\uparrow})(\tfrac{1}{2} - n_{i^{(b)}\downarrow}) + V \sum_{\langle i^{(b)}, j^{(b)}\rangle} (1 - n_{i^{(b)}})(1 - n_{j^{(b)}}) + k \sum_{i^{(b)}} I^{(b)}_i, \tag{5}$$

and the interblock interaction is

$$H_{b,b'} = -t \sum_{\langle i^{(b)}, j^{(b')}\rangle,\sigma} [c^{\dagger}_{i^{(b)}\sigma} c_{j^{(b')}\sigma} + \text{h.c.}] + V \sum_{\langle i^{(b)}, j^{(b')}\rangle} (1 - n_{i^{(b)}})(1 - n_{j^{(b')}}), \tag{6}$$

where $i^{(b)}$, $j^{(b)}$ are the labels of sites in the block $b$ and $\langle i^{(b)}, j^{(b')}\rangle$ denotes the interacting boundary sites, from neighboring blocks $b$ and $b'$.

In the EHM, the total particle number and spin are good quantum numbers; hence, the Hilbert space of each block can be separated into different subspaces according to $n^s$ and $S_z$. For a half-filled case, each block will have seven electrons on average. Due to fluctuations of the particle number on each block, we can divide the block Hilbert space into four subspaces, namely, $n^s = 6$ with three spins up and three spins down, $n^s = 7$ with four spins up and three spins down, $n^s = 7$ with three spins up and four spins down and $n^s = 8$ with four spins up and four spins down. Accordingly, the ground state for each subspace is expressed as

$$|\phi_{b1}\rangle \equiv |0\rangle'_b, \tag{7}$$

$$|\phi_{b2}\rangle \equiv c^\dagger_{b\uparrow}|0\rangle'_b = |\uparrow\rangle'_b, \tag{8}$$

$$|\phi_{b3}\rangle \equiv c^\dagger_{b\downarrow}|0\rangle'_b = |\downarrow\rangle'_b, \tag{9}$$

$$|\phi_{b4}\rangle \equiv c^\dagger_{b\uparrow\downarrow}|0\rangle'_b = |\uparrow\downarrow\rangle'_b, \tag{10}$$

where $c^\dagger_{b\sigma}$ ($c_{b'\sigma}$) is the creation (annihilation) operator of the block state $|\sigma\rangle'_b$. The corresponding energies are $\lambda_i$ ($i = 1, 2, 3, 4$). The above four states will be retained for each block, which could be directly mapped to the four states on each site in the original lattice, i.e., $|0\rangle$, $c^\dagger_{i\uparrow}|0\rangle \equiv |\uparrow\rangle$, $c^\dagger_{i\downarrow}|0\rangle \equiv |\downarrow\rangle$, $c^\dagger_{i\uparrow}c^\dagger_{i\downarrow}|0\rangle \equiv |\uparrow\downarrow\rangle$. In the notation introduced above, the renormalized block Hamiltonian $H_b$ can be approximately written as

$$\begin{aligned} H_b &= |0\rangle'_b\lambda_1\langle 0|'_b + |\uparrow\rangle'_b\lambda_2\langle\uparrow|'_b + |\downarrow\rangle'_b \\ &\quad\times \lambda_3\langle\downarrow|'_b + |\uparrow\downarrow\rangle'_b\lambda_4\langle\uparrow\downarrow|' \\ &= \lambda_1 - (\lambda_1-\lambda_2)n'_{b\uparrow} - (\lambda_1-\lambda_3)n'_{b\downarrow} \\ &\quad + (\lambda_1-\lambda_2-\lambda_3+\lambda_4)n'_{b\uparrow}n'_{b\downarrow}, \end{aligned} \tag{11}$$

by assuming the four states in equations (7)–(10) to form a complete set of states in the block Hilbert space. The particle–hole symmetry leads to $\lambda_2 = \lambda_3$. The new intersite Hamiltonian can be obtained as

$$\begin{aligned} H'_b &= (\lambda_1+\lambda_4-2\lambda_2)\sum_b n'_{b\uparrow}n'_{b\downarrow} - (\lambda_1-\lambda_2) \\ &\quad\times \sum_b (n'_{b\uparrow}+n'_{b\downarrow}) + \lambda_1\sum_b I_b. \end{aligned} \tag{12}$$

Comparing with equation (5), we can obtain the renormalized parameters $U'$, $\mu'$, and $k'$ as

$$U' = \lambda_1 + \lambda_4 - 2\lambda_2, \tag{13}$$

$$\mu' = \lambda_1 - \lambda_2, \tag{14}$$

$$k' = \lambda_1. \tag{15}$$

It should be mentioned that $\lambda_1$ and $\lambda_2$ are functions of the old parameters $t$, $U$, $V$, $K$.

By using similar procedures, we can get the renormalized intersite part $H_{b,b'}$,

$$\begin{aligned} H_{b,b'} &= -t \sum_{\langle i^{(b)}, j^{(b')}\rangle,\sigma,i_1,i'_1,i_2,i'_2} [|\psi_{bi_1}\rangle\langle\psi_{bi_1}|c^\dagger_{i^{(b)}\sigma}|\psi_{bi'_1}\rangle\langle\psi_{bi'_1}| \\ &\quad\times |\psi_{b'i_2}\rangle\langle\psi_{b'i_2}|c_{j^{(b')}\sigma}|\psi_{b'i'_2}\rangle\langle\psi_{b'i'_2}| + \text{h.c.}] \\ &\quad + V \sum_{\langle i^{(b)}, j^{(b')}\rangle,\sigma,i_1,i'_1,i_2,i'_2} [|\psi_{bi_1}\rangle\langle\psi_{bi_1}|(1-n'_{i^{(b)}})|\psi_{bi'_1}\rangle\langle\psi_{bi'_1}| \\ &\quad\times |\psi_{b'i_2}\rangle\langle\psi_{b'i_2}|(1-n'_{j^{(b')}})|\psi_{b'i'_2}\rangle\langle\psi_{b'i'_2}|] \end{aligned} \tag{16}$$

$$\begin{aligned} &= -t \sum_{\langle i^{(b)}, j^{(b')}\rangle,\sigma} \{\langle\sigma|'_b c^\dagger_{i^{(b)}\sigma}|0\rangle'_b + [\langle -\sigma,\sigma|'_b c^\dagger_{i^{(b)}\sigma}|-\sigma\rangle'_b \\ &\quad - \langle\sigma|'_b c^\dagger_{i^{(b)}\sigma}|0\rangle'_b]n'_{b-\sigma}\}c'^\dagger_{i^{(b)}\sigma}\{\langle 0|'_{b'}c_{j^{(b')}\sigma}|\sigma\rangle'_{b'} \\ &\quad + [\langle -\sigma|'_{b'}c_{j^{(b')}\sigma}|-\sigma,\sigma\rangle'_{b'} - \langle 0|'_{b'}c_{j^{(b')}\sigma}|\sigma\rangle'_{b'}]n'_{b'-\sigma}\}c'_{j^{(b')}\sigma} \\ &\quad + \text{h.c.} + V \sum_{\langle i^{(b)}, j^{(b')}\rangle,\sigma} (1 - \langle 0|'_b n_{i^{(b)}}|0\rangle'_b) \\ &\quad\times (1 - \langle 0|'_{b'}n_{j^{(b')}}|0\rangle'_{b'}). \end{aligned} \tag{17}$$

To keep $H_{b,b'}$ of the form

$$\begin{aligned} H_{b,b'} &= -t' \sum_{\langle i^{(b)}, j^{(b')}\rangle,\sigma} [c'^\dagger_{i^{(b)}\sigma}c'_{j^{(b')}\sigma} + \text{h.c.}] \\ &\quad + V' \sum_{\langle i^{(b)}, j^{(b')}\rangle} (1-n'_{i^{(b)}})(1-n'_{j^{(b')}}), \end{aligned} \tag{18}$$

we set

$$\langle -\sigma,\sigma|'_b c^\dagger_{i^{(b)}\sigma}|-\sigma\rangle'_b = \langle\sigma|'_b c^\dagger_{i^{(b)}\sigma}|0\rangle'_b, \tag{19}$$

$$\langle -\sigma|'_{b'}c_{j^{(b')}\sigma}|-\sigma,\sigma\rangle'_{b'} = \langle 0|'_{b'}c_{j^{(b')}\sigma}|\sigma\rangle'_{b'}. \tag{20}$$

Hence,

$$t' = \nu\zeta^2 t, \qquad \zeta = \langle -\sigma,\sigma|'_b c^\dagger_{i^{(b)}\sigma}|_b - \sigma\rangle'_b = \langle\sigma|'_b c'^\dagger_{i^{(b)}\sigma}|0\rangle'_b, \tag{21}$$

$$V' = \nu(1 - \langle 0|'n_i|0\rangle')^2 V, \tag{22}$$

where $\nu$ represents the number of couplings between neighboring blocks, which is 3 in our case. Equations (13)–(15) and equations (21) and (22) form a set of complete RG flow equations in the parameter space.

### 2.2. The Hartree–Fock approximation

The EHM can have CDW and SDW phases. But it is difficult to apply the BRG method to investigate these phases since a bigger block is needed in order to support the corresponding low-energy waves. In order to solve this problem, we will try to make use of the Hartree–Fock approximations, which can reduce the many-body problem into a set of single-body ones by decoupling interactions through mean fields. For the EHM, the on-site interactions can be approximated as

$$\begin{aligned} H_U &\simeq U\sum_i [\langle n_{i\uparrow}\rangle n_{i\downarrow} + n_{i\uparrow}\langle n_{i\downarrow}\rangle - \langle n_{i\uparrow}\rangle\langle n_{i\downarrow}\rangle \\ &\quad - \langle c^\dagger_{i\downarrow}c_{i\uparrow}\rangle c^\dagger_{i\downarrow}c_{i\uparrow} - \langle c^\dagger_{i\uparrow}c_{i\downarrow}\rangle c^\dagger_{i\uparrow}c_{i\downarrow} + \langle c^\dagger_{i\uparrow}c_{i\downarrow}\rangle\langle c^\dagger_{i\downarrow}c_{i\uparrow}\rangle], \end{aligned} \tag{23}$$

and the nearest-neighbor interactions as

$$\begin{aligned} H_V &\simeq V\sum_{\langle i,j\rangle} [\langle n_i\rangle n_j + n_i\langle n_j\rangle - \langle n_i\rangle\langle n_j\rangle - \langle c^\dagger_{i\uparrow}c_{j\uparrow}\rangle c^\dagger_{j\uparrow}c_{i\uparrow} \\ &\quad - \langle c^\dagger_{j\uparrow}c_{i\uparrow}\rangle c^\dagger_{i\uparrow}c_{j\uparrow} + \langle c^\dagger_{i\uparrow}c_{j\uparrow}\rangle\langle c^\dagger_{j\uparrow}c_{i\uparrow}\rangle \end{aligned}$$

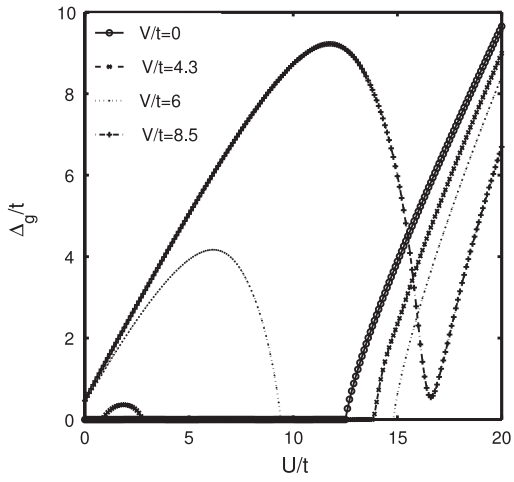


**Figure 2.** Variations of the charge gap $\Delta_g/t$ against the on-site interactions $U/t$ with fixed values of $V/t$.

$$- \langle c^{\dagger}_{i\uparrow} c_{j\downarrow}\rangle c^{\dagger}_{j\downarrow} c_{i\uparrow} - \langle c^{\dagger}_{j\downarrow} c_{i\uparrow}\rangle c^{\dagger}_{i\uparrow} c_{j\downarrow} + \langle c^{\dagger}_{i\uparrow} c_{j\downarrow}\rangle \langle c^{\dagger}_{j\downarrow} c_{i\uparrow}\rangle$$
$$- \langle c^{\dagger}_{i\downarrow} c_{j\uparrow}\rangle c^{\dagger}_{j\uparrow} c_{i\downarrow} - \langle c^{\dagger}_{j\uparrow} c_{i\downarrow}\rangle c^{\dagger}_{i\downarrow} c_{j\uparrow} + \langle c^{\dagger}_{i\downarrow} c_{j\uparrow}\rangle \langle c^{\dagger}_{j\uparrow} c_{i\downarrow}\rangle$$
$$- \langle c^{\dagger}_{i\downarrow} c_{j\downarrow}\rangle c^{\dagger}_{j\downarrow} c_{i\downarrow} - \langle c^{\dagger}_{j\downarrow} c_{i\downarrow}\rangle c^{\dagger}_{i\downarrow} c_{j\downarrow} + \langle c^{\dagger}_{i\downarrow} c_{j\downarrow}\rangle \langle c^{\dagger}_{j\downarrow} c_{i\downarrow}\rangle], \tag{24}$$

where the minus signs follow from fermionic statistics and $\langle \cdots \rangle$ denotes the average over the mean-field wavefunctions. Following the general steps of mean-field theory, we firstly initialize the mean-field parameters $\langle \cdots \rangle$ in equations (23) and (24). Next, the initialized Hamiltonian is solved numerically to get all of its eigenvalues $\varepsilon_l(i,\sigma)$ and eigenvectors $\phi_l(i,\sigma)$. For an $n \times n$ cluster, we need to diagonalize a $2n^2 \times 2n^2$ matrix. Then, the eigenvectors obtained are used to acquire the charge density and magnetization component,

$$\langle n_{i,\sigma}\rangle = \sum_{|\varepsilon_l < E_F|} |\phi_l(i,\sigma)|^2, \tag{25}$$

$$\langle c^{\dagger}_{i\sigma} c_{j\sigma'}\rangle = \sum_{|\varepsilon_l < E_F|} |\phi_l(i,\sigma)\phi_l(j,\sigma')|, \tag{26}$$

where the lowest $n^2$ eigenvectors are filled for the half-filled case with $E_F$ the corresponding Fermi energy. Finally, equations (25) and (26) are fed back into equations (23) and (24) to get the new Hamiltonian. Then we iterate the above three steps until convergence is achieved. It might be noted that only a fraction of the mean-field parameters in equations (23) and (24) will be updated for each iteration. This relaxation technique is necessary in order to guarantee convergence, which depends sensitively on the initial conditions.

## 3. Results and discussion

### *3.1. The MIT*

The charge gap $\Delta_g$ is an order parameter used to determine whether a system is in a metallic or a Mott insulating state, which is defined as

$$\Delta_g = E(N_e - 1) + E(N_e + 1) - 2E(N_e), \tag{27}$$

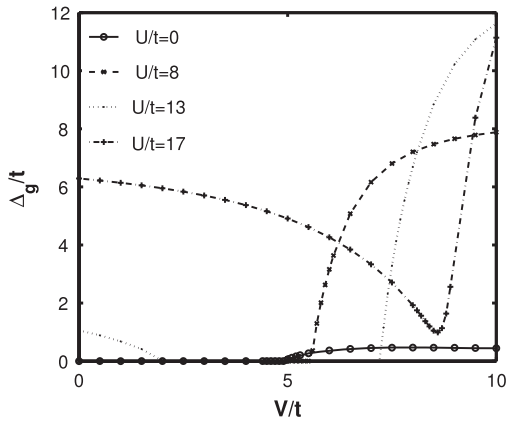


**Figure 3.** The same as figure 2 but for the nearest-neighbor interactions $V/t$ with fixed values of $U/t$.

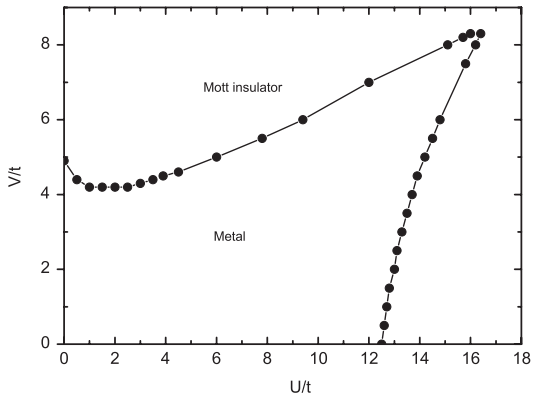


**Figure 4.** The MIT phase diagram of the EHM on a triangular lattice.

where $E(N_e)$ denotes the lowest energy for the $N_e$ electron system. If $\Delta_g = 0$, the systems exhibits metallic behavior. Otherwise it is insulating. Lieb and Mattis [21] have proved that, for an electronic system with arbitrary symmetrical potential, the absolute ground-state energy lies within the $S = |S_z|$ subspace, where, for a given electron number $N$, $|S_z|$ takes the lowest possible value. Hence, for a seven-site block, the ground state of seven electrons will lie in the subspace with four spins up and three spins down or vice versa, which means $E(7) = \lambda_2$. Similarly, $E(6) = \lambda_1$ and $E(8) = \lambda_4$. The corresponding charge gap is then equal to $\lambda_1 + \lambda_4 - 2\lambda_2$. Comparing with equation (13), equation (27) can be expressed as

$$\Delta_g = \lim_{n\to\infty} U^{(n)}, \tag{28}$$

where $n$ denotes the order of the iterations in equation (13).

In our calculations, all the energy will be scaled in units of $t$. In figure 2, we plot the order parameter $\Delta_g$ as a function of $U/t$ for different values of $V/t$. It is obvious that as $V = 0$, the EHM reduces to the HM and the MIT happens at a finite on-site interaction, i.e. $U/t = 12.5$, which is consistent with the exact-diagonalization result for a 12-site lattice with $U/t = 12.07$ [6]. As $V/t$ is larger than zero, it is interesting to note that the Mott insulator near the

transition point becomes unstabilized against the metallic state, namely, we need higher on-site interaction in order to observe the MIT. In other words, the nearest-neighbor interactions are actually reducing the effective on-site interactions. This can be understood by realizing that the occupation of two electrons on one site is more favored by $V/t$ than the distribution of two electrons on two sites favored by $U/t$. This phenomenon will continue until $V/t = 4.2$. Then there is a striking effect, namely, in the metallic part of the parameter space of $U/t$, we can observe an island of Mott insulating region. Hence there are now three MIT critical points. The first is from a metallic to an insulating state and the second is the re-entrance of the insulator to the metal. Finally, the system goes to insulator again. This phenomenon might be related to the CDW instabilities since the metallic state originates from the high spin degeneracy in the frustrated triangular lattice and the CDW tends to lift the degeneracy, which could then drive the system into an insulator in the metallic region. Generally speaking, while $V/t$ is increased, the region of Mott phase will expand until the left MIT critical point touches the axis with $U/t = 0$, which happens around $V/t = 4.4$. If $V/t$ is further increased beyond 4.4, there are two MIT critical points left and the insulating region keeps expanding until finally the right MIT critical point leaves the $U/t$ axis around $V/t = 8.4$ and the system is insulating for all values of $U/t$.

Figure 3 presents the results for the charge gap against $V/t$ for different $U/t$ values. A phenomenon similar to that in figure 2 is seen, i.e., the MIT emerges at a finite value of $V/t$ when $U/t = 0$. And when $U/t$ is large enough, the metallic phase disappears. The difference in behavior from figure 2 is that, as $U/t$ is increased, the charge gap opens not in the middle part along the $V/t$ axis, but directly from the border at $V/t = 0$. Hence we can only observe two critical points before the whole system transforms into an insulating state.

Collecting all the data in figures 2 and 3, we present the full MIT phase diagram in figure 4, from which we can clearly see the general features of the MIT in the EHM. When both $U/t$ and $V/t$ are small, the system is in a metallic phase due to the frustration effect. In the case with $U/t \to \infty$ or $V/t \to \infty$, it is in a Mott insulating state due to the strong electron repulsions and the resulting localized states. The richest phase transitions happen when $U/t$ and $V/t$ are competing with each other, which has been explained above. Moreover, from figure 4, we can notice another interesting effect. In the region of $4.2 \leqslant V/t \leqslant 4.4$, a small on-site interaction will firstly lower the critical value of $V/t$ and then increase it. If we renormalize $U/t$ into $V/t$, we can say that the on-site interaction tends to first increase and then decrease the effective nearest-neighboring interactions. This is in direct comparison with what happens along the $U/t$ axis, in which the nearest-neighbor interactions can only decrease the effective $U$. These effects have demonstrated clearly the subtlety of the competition effect from on-site and nearest-neighbor interactions upon the MIT.

### 3.2. Finite size scaling analysis

In order to understand the universality class of the MIT happening in the EHM, in this section, we introduce the finite size scaling analysis. In the RG calculations, if the iteration is stopped at different step, we can get the size dependence of the charge gap. As an example, in figure 10(a), we present the size dependence of $\Delta_g$ upon $V/t$ at $U/t = 0$. In figure 10(b), $\Delta_g$ is scaled with respect to $N$. The crossing point corresponds to the critical value $(V/t)_c = 4.95$. Moreover, in figure 10(c), all the data can collapse to one curve once a rescaling of $V/t$ with $N$ is used. The above finite size scaling can be compactly expressed as

$$\Delta_g N^{0.405} = f[qN^{0.63}], \tag{29}$$

where $f(x)$ is a universal function independent of the system size and $q = V/t - (V/t)_c$. By using $N = L^2$ for a 2D system, the above equation can be changed to

$$\Delta_g = L^{-0.81} f[qL^{1.26}]. \tag{30}$$

According to the one-parameter scaling theory, we have

$$\Delta_g = q^{y_\Delta} f[L/\xi], \tag{31}$$

in which $\xi = q^{-\nu}$ is the correlation length with $\nu$ being the corresponding critical exponent and $L$ denotes the system size. Comparing with equation (29), it can be obtained that

$$y_\Delta = 0.643, \qquad \nu = 0.794. \tag{32}$$

There is a relationship between $y_\Delta$ and the dynamic critical exponent $z$, namely, $y_\Delta = z\nu$. Hence $z = 0.81$. Through similar procedures, the critical exponents at other critical points in the MIT phase diagram can also be obtained. After intensive calculations, we find that the MIT induced by $V$ has the same critical exponent $\nu = 0.794$ and $z = 0.81$. For the phase transition induced by $U$, $\nu = 1$ and $z = 0.81$, the same as early results from the real space method [8]. Different critical exponents imply different underlying mechanisms of the MIT. In our model, they are just the on-site and nearest-neighbor interactions.

### 3.3. The SDW and CDW

The competition of the short- and long-range interactions not only emerges in the MIT, but also happens in the SDW and CDW. To characterize the SDW and CDW phases, we calculate the spin and the charge structure factors in the momentum space by using

$$S(\mathbf{k}) = \frac{1}{N^2}\sum_{ij}\langle n_{i\uparrow} - n_{i\downarrow}\rangle\langle n_{j\uparrow} - n_{j\downarrow}\rangle e^{i\mathbf{k}(\mathbf{r_i}-\mathbf{r_j})}, \tag{33}$$

and

$$C(\mathbf{k}) = \frac{1}{N^2}\sum_{ij}\langle n_i\rangle\langle n_j\rangle e^{i\mathbf{k}(\mathbf{r_i}-\mathbf{r_j})}, \tag{34}$$

respectively, where the average values of $\langle\cdots\rangle$ are given by equations (25) and (26). A $12 \times 12$ system with periodic boundary conditions is used in the following calculations.

Some examples of SDW order (SO) are presented in figures 5(a)–(c) with $V/t = 0$. It is easy to see that when $U/t = 3$, $S(\mathbf{k})$ is zero, independently of $\mathbf{k}$. When $U/t$ is increased to 7, there emerge some peaks, indicating the

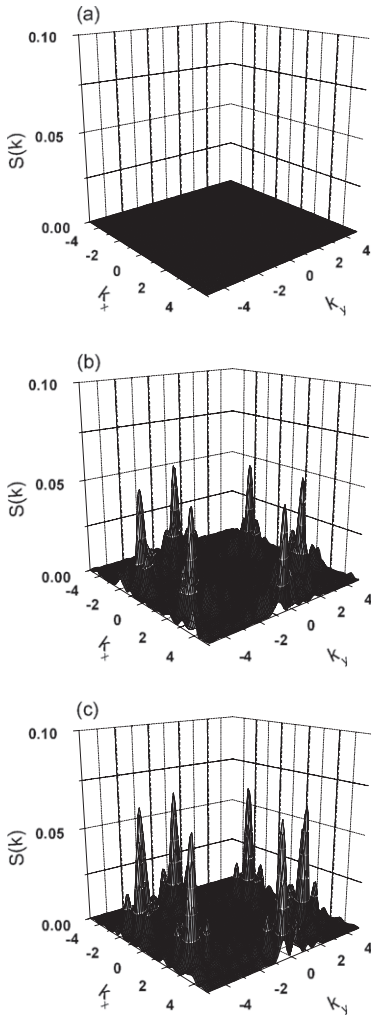


**Figure 5.** Spin structure factor $S(\mathbf{k})$ in the momentum space for different $U/t$ values with $V/t = 0$ ($U/t = 3$ (a), $U/t = 7$ (b), $U/t = 11$ (c)).

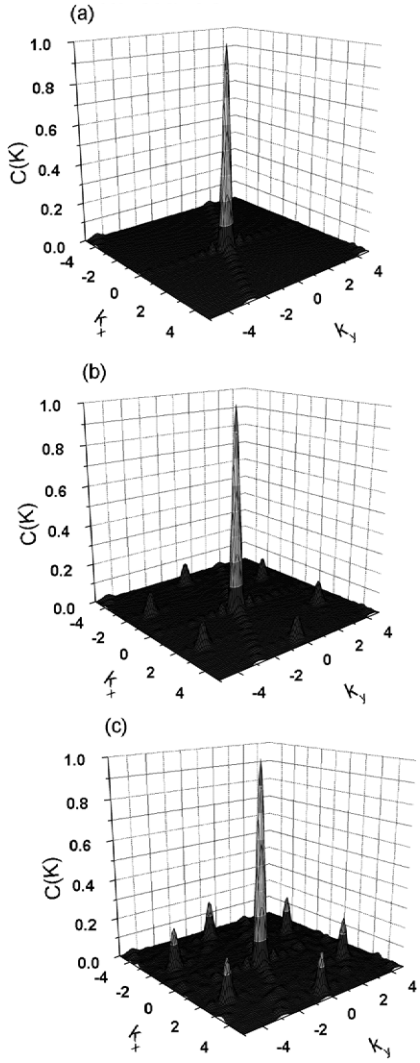


**Figure 6.** The same as figure 5, but for the charge structure factor $C(\mathbf{k})$ with different $V/t$ values and fixed $U/t = 0$ ($V/t = 0.6$ (a), $V/t = 1.2$ (b), $V/t = 3.0$ (c)).

appearance of SO. Hence there exists a critical value of $U/t$ for SO to emerge. As $U/t$ is increased to 11, more peaks appear. By careful observations, we find that the highest peaks always sit upon some fixed points, namely, $(\pm 4\pi/3, 0)$ and $(\pm 2\pi/3, \pm 2\pi/\sqrt{3})$, which exactly correspond to the symmetry axes of the triangular lattice. Similar examples used to demonstrate the features of the CDW order (CO) are given in figure 6. The same phenomenon is observed. Thus, for a 2D frustrated structure, $U/t$ and $V/t$ tend to induce the SO and CO, respectively, just as for 1D and 2D non-frustrated cases. To find the details of how the SDW and CDW compete with each other, the variations of the maximum values of $S(\mathbf{k})$ and $C(\mathbf{k})$ at the point $(\pm 4\pi/3, 0)$ against $U/t$ for different $V/t$ values are given in figures 7(a)–(c). Figure 7(a) is for $V/t = 0$, in which $C(\mathbf{k})$ remains zero for all values of $U/t$, meaning nonexistence of CO in this parameter region. But for SO, there is a phase transition at finite critical on-site interactions, i.e., $U/t = 6$. The case with $V/t = 1.5$ is shown in figure 7(b), in which the competition between SO and CO is obvious. When $0 \leqslant U/t \leqslant 4$, the CO exists without SO. Then as $U/t \geqslant 4$, the CO becomes unstable and disappears. As $U/t$ is further increased until $U/t = 6.5$, the SO appears. In the region with $0 \leqslant U/t \leqslant 4$, there seems to be a crossover regime in which neither SO nor CO exists. It is also interesting to note that when $V/t$ is large enough, for example $V/t = 3$ as shown in figure 7(c), the crossover regime disappears and the phase transition happens directly, between SO and CO. Similarly, when we keep $U/t$ fixed and study the dependence of the CO and SO upon $V/t$, the same results are obtained except that the role of CO and SO needs to be exchanged. This is shown in figures 8(a)–(c). One thing that needs to be mentioned is that, at $U/t = 5$, CO emerges at $V/t = 1.8$, which is in agreement with the work of Davoudi [22] using the extended two-particle self-consistent approach, which in some way shows the reliability of the results presented here. Figure 9 summarizes the phase diagram of SO and CO in the metallic region. Just as in [23], within the framework of the slave-boson technique, the coexistence of CO and SO has not been found in our work either. Moreover, we can clearly see from figure 9 that an instability of SO driven by $V/t$ exists

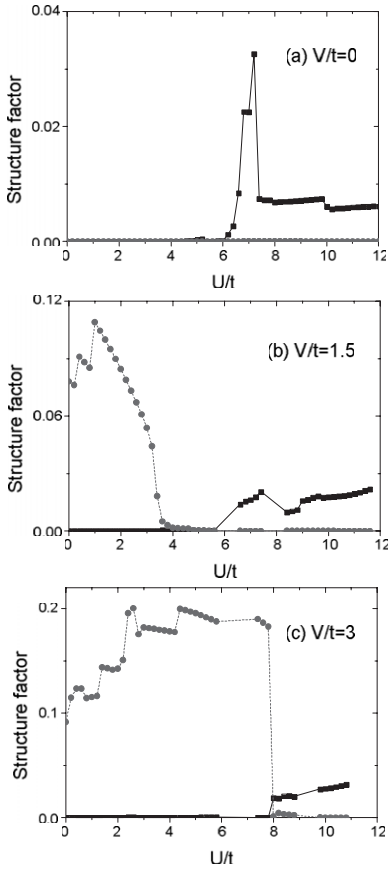


**Figure 7.** Variation of the spin (solid line) and charge (dotted line) structure factors against $U/t$ for different $V/t$ values.

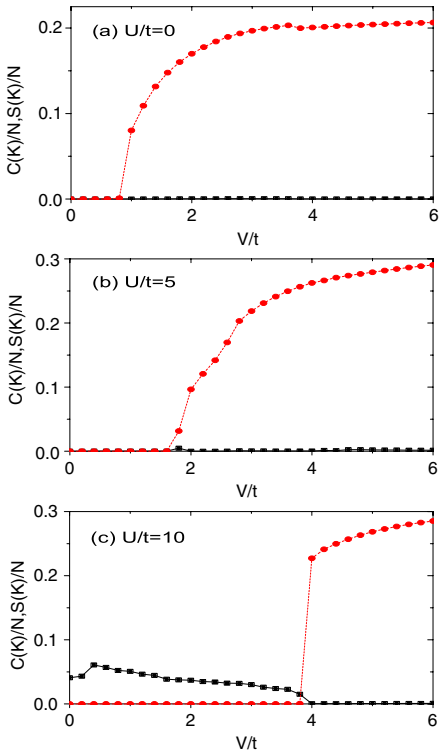


**Figure 8.** The same as figure 7, but for fixed $U/t$ while tuning $V/t$. (This figure is in colour only in the electronic version)

before the appearance of CO when $U/t$ is between 5 and 8. This phenomenon is also consistent with those given in [23]. But comparing with the 1D case [23], the 2D frustrated system seems to be much more complex since a region without CO and SO can be observed when the repulsions $V/t$ and $U/t$ are not strong enough. Unfortunately, we cannot give the phase diagram in the full parameter space due to the convergence problem of the HFA, which might imply that new mean-field order parameters are needed.

### *3.4. Entanglement*

Recently much work has shown that entanglement can be used to characterize a quantum phase transition [19]. For spin models, the entanglement of two neighboring sites displays a sharp peak at the critical point where the quantum phase transition takes place [24, 25]. For the fermionic systems, Gu and Deng [26] have demonstrated that entanglement can be used as a unique quantity for describing quantum phase transitions, and Daniel [27] has put forward a single-site entanglement to be used as a reliable mark of the MIT in the 1D HM. In order to decide whether the single-site entanglement can give consistent results in identifying the MIT in our model, we use the BRG method to carry out the investigations. The details of the procedure can be found in [28]

For fermionic systems, von Neuman entropy is usually used to measure the entanglement, which is defined as

$$E_j = -\operatorname{Tr}[\rho_j \ln_2 \rho_j], \qquad \rho_j = \operatorname{Tr}_j |\Omega\rangle\langle\Omega|, \tag{35}$$

where $\operatorname{Tr}_j$ denotes the trace over all the unwanted freedoms and $\Omega$ is the antisymmetric wavefunction of the system studied.

For the single-site entanglement, only one site freedom will be kept and all the others need to be traced out. Generally, the local density matrix $\rho_i$ for the $i$th site can be written as

$$\rho_i = z_i|0\rangle\langle 0| + u_i^{\dagger}|\uparrow\rangle\langle\uparrow| + u_i^{-}|\downarrow\rangle\langle\downarrow| + w_i|\uparrow\downarrow\rangle\langle\uparrow\downarrow|, \tag{36}$$

where

$$w_i = \langle n_{i\uparrow} n_{i\downarrow}\rangle, \tag{37}$$

$$u_i^{\dagger} = \langle n_{i\uparrow}\rangle - w_i, \tag{38}$$

$$u_i^{-} = \langle n_{i\downarrow}\rangle - w_i, \tag{39}$$

$$z_i = 1 - \langle n_{i\uparrow}\rangle - \langle n_{i\downarrow}\rangle + w_i, \tag{40}$$

from which we can get

$$E_v^i = -u_i^{\dagger}\log_2 u_i^{\dagger} - u_i^{-}\log_2 u_i^{-} - w_i \log_2 w_i - z_i \log_2 z_i. \tag{41}$$

Normally, the size effect cannot be neglected and $E_v^i$ depends on $i$. Hence without loss of generality, the average value of

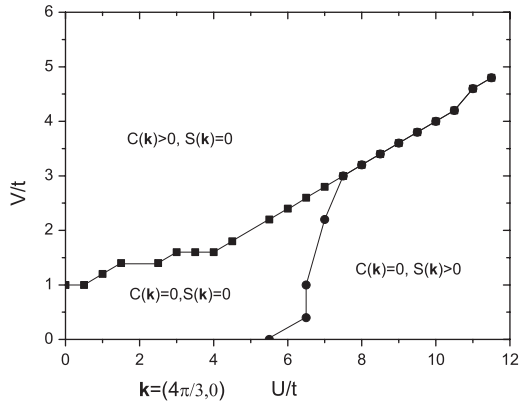


**Figure 9.** The phase diagram for SDW and CDW phases in the metallic regime of the EHM, as shown in figure 4.

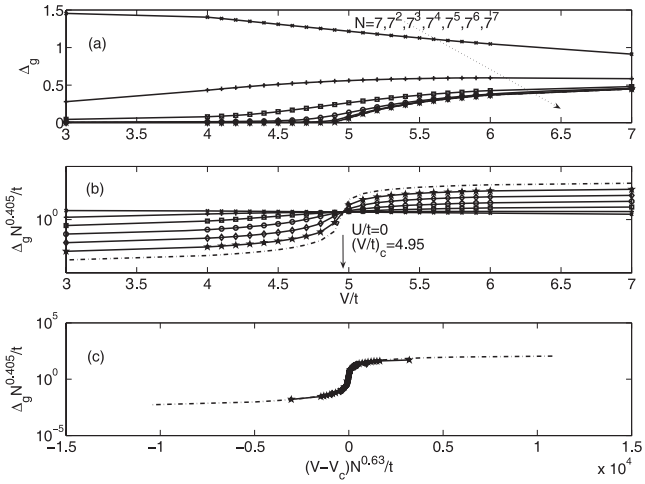


**Figure 10.** The finite size scaling of the charge gap against $V/t$.

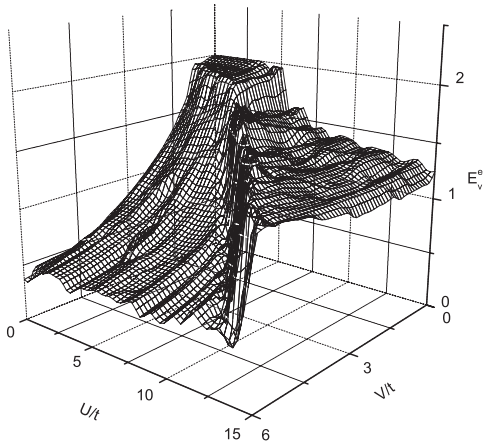


**Figure 11.** Variation of the single-site entanglement in the parameter space $U/t$, $V/t$, obtained from the HFA.

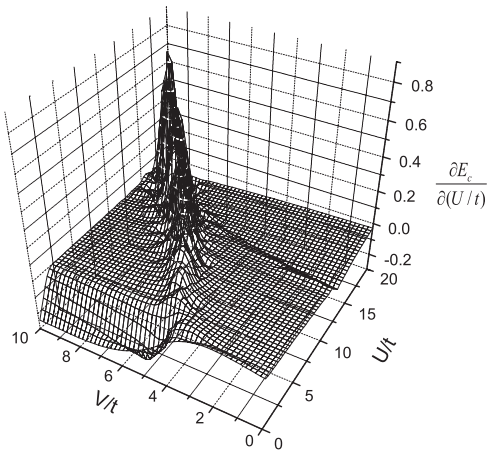


**Figure 12.** The same as figure 11, but for the derivative of the entanglement obtained from the BRG.

the von Neumann entropy [29] will be used:

$$E_v^e = \frac{1}{N}\sum_i (-u_i^\dagger \log_2 u_i^\dagger - u_i^- \log_2 u_i^- - w_i \log_2 w_i - z_i \log_2 z_i). \quad (42)$$

With the HFA, due to the size effect, we need to calculate the average single-site entanglement. The results are given in figure 11, from which we can clearly observe the jump of the entanglement along the critical line of the MIT. This implies that the metal and insulating phases have quite different kinds of many-body correlations.

In the BRG method, the entanglement can also be calculated [30]. And the size effect is not a serious problem. So the entanglement between the central site and all the others is just what we want. As a lot of work has shown before, the derivative of the entanglement with respect to the order parameter is sometimes more suitable for revealing the quantum phase transitions. Hence in figure 12, the variations of the entanglement derivative with respect to the order parameter $U/t$ are presented. Comparing with the phase diagram in figure 4, it can be found that the extremum of the entanglement derivative also follows well the critical line of the MIT. And specifically, the phase border line can be separated into two sections. One section corresponds to the maximum value and the second one to the minimum value.

## 4. Summary

In this paper, by using the BRG method and a mean-field technique based upon the HFA, we have investigated in detail the MIT in the half-filled extended Hubbard model on a triangular lattice. The main results that we have obtained can be summarized as follows.

(1) The MIT can be driven by either the finite on-site interactions or the nearest-neighbor ones, but with different critical exponents $\nu$. For the MIT induced by $U/t$ while keeping $V/t$ fixed, we have $\nu = 1, z = 0.81$. But if the MIT is induced by $V/t$ with $U/t$ fixed, $\nu = 0.794, z = 0.81$.

(2) When both $U/t$ and $V/t$ are small, the system shows metallic behavior due to the frustrated lattice structure. And if the electron repulsions are strong enough, the system will be in an insulating state due to the interaction-induced localizations.

(3) For $V/t \leqslant 4.2$, there is one critical point for the MIT with respect to $U/t$. When $4.2 \leqslant V/t \leqslant 4.4$ or $V/t \geqslant 8.4$, there are three and two critical points, respectively. If $V/t \geqslant 8.4$, no MIT exists.
(4) In the metallic regime, the SDW and CDW phases have been studied using mean-field theory based upon Hartree–Fock approximations. According to the structure factors in the momentum space, we can divide the metallic regime in the phase diagram into different parts and find that the nearest-neighbor interaction $V/t$ can induce CO, which then leads to complicated phase structure when it is competing with the SO induced by $U/t$.
(5) The single-site entanglement has also been calculated. Its first derivative with respect to $U$ demonstrates an extremum along the MIT critical line.

## Acknowledgment

This work is supported by the National Basic Research Program of China (973 program) under Grant No. 2006CB921104.

## References

[1] Kravchenko S V, Kravchenko G V, Furneaux J E, Pudalov V M and D'Iorio M 1994 Possible metal–insulator transition at $b = 0$ in two dimensions *Phys. Rev.* B **50** 8039–42
[2] Abrahams E, Kravchenko S V and Sarachik M P 2001 Metallic behavior and related phenomena in two dimensions *Rev. Mod. Phys.* **73** 251–66
[3] Jeckelmann E 2002 Ground-state phase diagram of a half-filled one-dimensional extended Hubbard model *Phys. Rev. Lett.* **89** 236401
[4] Merino J, Powell B J and McKenzie R H 2006 Ferromagnetism, paramagnetism, and a Curie–Weiss metal in an electron-doped Hubbard model on a triangular lattice *Phys. Rev.* B **73** 235107
[5] Mott N F 1974 *Metal Insulator Transitions* (London: Taylor and Francis)
[6] Capone M, Capriotti L, Becca F and Caprara S 2001 Mott metal–insulator transition in the half-filled Hubbard model on the triangular lattice *Phys. Rev.* B **63** 085104
[7] Powell B J and McKenzie R H 2005 Half-filled layered organic superconductors and the resonating-valence-bond theory of the Hubbard–Heisenberg model *Phys. Rev. Lett.* **94** 047004
[8] Wang J X and Kais S 2002 Finite-size scaling for Mott metal–insulator transition on a half filled nonpartite lattice *Phys. Rev.* B **66** 081101
[9] Takada K, Sakurai H, Takayama-Muromachi E, Izumi F, Dilanian R A and Sasaki T 2003 Superconductivity in two-dimensional $CoO_2$ layers *Nature* **422** 53–5
[10] Foo M L, Wang Y, Watauchi S, Zandbergen H W, He T, Cava R J and Ong N P 2004 Charge ordering, commensurability, and metallicity in the phase diagram of the layered $Na_xCoO_2$ *Phys. Rev. Lett.* **92** 247001
[11] White S R, Scalapino D J, Sugar R L, Loh E Y, Gubernatis J E and Scalettar R T 1989 Numerical study of the two-dimensional Hubbard model *Phys. Rev.* B **40** 506–16
[12] Sénéchal D, Perez D and Pioro-Ladrière M 2000 Spectral weight of the Hubbard model through cluster perturbation theory *Phys. Rev. Lett.* **84** 522–5
[13] Levine R D, Wang J X and Kais S 2002 Real-space renormalization group study of the Hubbard model on a non-bipartite lattice *Int. J. Mol. Sci.* **3** 69
[14] Vergés J A, Louis E, Lomdahl P S, Guinea F and Bishop A R 1991 Holes and magnetic textures in the two-dimensional Hubbard model *Phys. Rev.* B **43** 6099–108
[15] Normand B and Kampf A P 2001 Lattice anisotropy as the microscopic origin of static stripes in cuprates *Phys. Rev.* B **64** 024521
[16] Tsai S W and Marston J B 2001 $\kappa$–$(BEDT\text{-}TTF)_2X$ organic crystals: superconducting versus anti-ferromagnetic instabilities in the Hubbard model on an anisotropic triangular lattice *Can. J. Phys.* **79** 1463–7
[17] Honerkamp C 2003 Instabilities of interacting electrons on the triangular lattice *Phys. Rev.* B **68** 104510
[18] Wang J and Kais S 2003 Combined effects of disorders and electron–electron interactions upon metal–insulator transition in 2D non-bipartite lattice *Phys. Lett.* **316** 265
[19] Amico L, Fazio R, Osterloh A and Vedral V 2008 Entanglement in many-body systems *Rev. Mod. Phys.* **80** 517
[20] Wilson K G and Kogut J 1974 The renormalization group and the $\epsilon$ expansion *Phys. Rep.* **12** 75–199
[21] Lieb E and Mattis D 1962 Theory of ferromagnetism and the ordering of electronic energy levels *Phys. Rev.* **125** 164–72
[22] Davoudi B, Hassan S R and Tremblay A-M S 2008 Competition between charge and spin order in the t–u–v extended Hubbard model on the triangular lattice *Phys. Rev.* B **77** 214408
[23] Caprara S, Avignon M and Sarma D D 1997 Spin and charge density waves in the extended Hubbard model: a slave boson approach *Int. J. Mod. Phys.* B **11** 2057
[24] Osterloh A, Amico L, Falci G and Fazio R 2002 Scaling of entanglement close to a quantum phase transition *Nature* **416** 608–10
[25] Osborne T J and Nielsen M A 2002 Entanglement in a simple quantum phase transition *Phys. Rev.* A **66** 032110
[26] Gu S-J, Deng S-S, Li Y-Q and Lin H-Q 2004 Entanglement and quantum phase transition in the extended Hubbard model *Phys. Rev. Lett.* **93** 086402
[27] Larsson D and Johannesson H 2006 Single-site entanglement of fermions at a quantum phase transition *Phys. Rev.* A **73** 042320
[28] Wang J and Kais S 2004 Scaling of entanglement at a quantum phase transition for a two-dimensional array of quantum dots *Phys. Rev.* A **70** 022301
[29] Zhu X and Tong P 2008 Quantum phase transition and von Neumann entropy of quasiperiodic Hubbard chains *Chin. Phys.* B **17** 1623–8
[30] Wang J and Kais S 2003 Scaling of entanglement in finite array of exchange-coupled quantum dots *Int. J. Quantum Inf.* **1** 375